JOURNAL OF GEOPHYSICAL RESEARCH, VOL. 107, NO. D19, 8009, 10.1029/2000JD000182, 2002

Aerosol optical depths and direct radiative forcing for INDOEX derived from AVHRR: Theory

James A. Coakley Jr. and William R. Tahnk
College of Oceanic and Atmospheric Sciences, Oregon State University, Corvallis, Oregon, USA

A. Jayaraman
Planetary Atmospheric Sciences Division, Physical Research Laboratory, Navrangpura, Ahmedabad, India

Patricia K. Quinn
NOAA/Pacific Marine Environmental Laboratory, Seattle, Washington, USA

Claude Devaux and Didier Tanré
Laboratoire d'Optique Atmosphérique, CNRS, Université des Sciences et Technologies de Lille, Villleneuve d'Ascq, France

Received 20 November 2000; revised 13 July 2001; accepted 12 November 2001; published 20 August 2002.

[1] A scheme is presented for retrieving aerosol properties for ocean regions from reflected sunlight at both the visible and near infrared wavelengths measured by the NOAA advanced very high resolution radiometer (AVHRR). For the Indian Ocean Experiment (INDOEX), aerosols were presumed to be a mixture of a continental haze that had small particles, contained soot, and absorbed sunlight, and a marine haze that had large particles and absorbed practically no sunlight. Because of the difference in particle sizes, the two aerosols reflect sunlight differently at visible and near infrared wavelengths. Reflectances at visible and near infrared wavelengths were thus used to determine mixing fractions for the continental and marine aerosols and the optical depth of the aerosol mixture. The fractions and optical depths along with the optical properties of the aerosols were then used in radiative transfer calculations to estimate the diurnally averaged top of the atmosphere and surface aerosol direct radiative forcing for ocean regions. Comparison of retrieved optical depths at visible and near infrared wavelengths with surface measurements revealed that several different retrieval schemes employing a variety of aerosol types provided comparable levels of agreement, but none of the aerosol models or retrieval schemes produced ratios of the near infrared to visible optical depths that agreed with the ratios obtained with the surface measurements. In estimating the top of the atmosphere radiative forcing, errors in the retrieved optical depths were in some cases found to be partially compensated by the effect of the aerosol on the radiative flux. For example, different aerosol models led to retrieved optical depths that differed by as much as 60%, but the top of the atmosphere forcing obtained with the models differed by less than 35% for cloud-free conditions. When aerosols absorb sunlight, there is no comparable compensation for the surface forcing. Cloud conditions contribute sizable uncertainties to estimates of the aerosol direct radiative forcing. For INDOEX, estimates of the aerosol direct radiative forcing for average cloud conditions were obtained by (1) setting the forcing to zero for all $1^\circ \times 1^\circ$ latitude-longitude boxes that contained any amount of upper-level cloud; (2) ascribing to regions with upper-level clouds the radiative forcing obtained for regions having only low-level clouds and, (3) setting the forcing to zero for all regions containing upper-level clouds and all portions of regions overcast by low-level clouds. Relative differences in the extreme values for the top of the atmosphere aerosol direct radiative forcing were less than 50%, but for the surface, the relative differences of the extreme values reached 70%. *INDEX TERMS:* 0305 Atmospheric Composition and Structure: Aerosols and particles (0345, 4801); 1640 Global Change: Remote sensing; 3359 Meteorology and Atmospheric Dynamics: Radiative processes; 3360 Meteorology and Atmospheric Dynamics: Remote sensing; *KEYWORDS:* INDOEX, aerosols, aerosol optical depth, remote sensing of aerosols, radiative forcing of climate

0148-0227/02/2000JD000182$09.00

1. Introduction

[2] A primary objective of the Indian Ocean Experiment (INDOEX) was the determination of the aerosol radiative forcing for the Indian Ocean during the January–March winter monsoon. Estimates of aerosol burdens and the consequent radiative forcing derived from satellite imagery data were the primary means for achieving this objective, and the advanced very high resolution radiometer (AVHRR) on the NOAA-14 satellite was a major source of observations. Several schemes have been devised for retrieving aerosol properties from AVHRR observations [*Durkee et al.*, 1991; *Stowe et al.*, 1997; *Higurashi and Nakajima*, 1999; *Mischenko et al.*, 1999; *Rajeev et al.*, 2000]. The schemes are identical in that aerosol properties are derived from the departures of the observed visible and near infrared reflectances from those expected for cloud-free and aerosol-free ocean scenes. The reflectances against which the observations are compared are obtained through radiative transfer calculations for a prescribed set of aerosol models. The schemes differ in the methods used to identify cloud-free ocean scenes suitable for the retrieval of aerosol properties, the models used for the ocean surface reflectance, and the aerosol models used to calculate the radiances expected for a cloud-free ocean. This study explores the sensitivity of the retrieved aerosol properties and the resulting estimates of the aerosol direct radiative forcing to various aerosol models used in several different retrieval schemes.

[3] Aerosol properties were derived from the NOAA-14 AVHRR observations using the results of radiative transfer calculations for the following aerosol models: (1) the tropical marine and average continental aerosols described by *Hess et al.* [1998]; (2) the model derived from aerosol composition and particle sizes deduced from data collected at the Kaashidhoo Climate Observatory (KCO) [*Satheesh et al.*, 1999] and used by *Rajeev et al.* [2000] to derive aerosol burdens and in a slightly revised form to estimate the radiative forcing for the INDOEX region [*Ramanathan et al.*, 2001]; this model will be referred to as the First Field Phase (FFP) model, and (3) the models used in the NOAA Phase 1 and Phase 2 operational algorithms [*Stowe et al.*, 1997]. In the case of the tropical marine and average continental aerosols, a new retrieval scheme was developed in which reflectances at visible (0.64-μm AVHRR Channel 1) and near infrared (0.84-μm AVHRR Channel 2) wavelengths were used to derive: (1) the fraction of the two aerosol components contributing to a mixed aerosol, and (2) the resulting optical depth of the mixture. This scheme is similar to that suggested by *Wang and Gordon* [1994] for retrievals that employ multiangle and multispectral observations, like MISR, and also by *Kahn et al.* [2001]. These schemes offer a plausible link between aerosol size and optical properties by mixing aerosol types with distinctive sizes and optical properties. This type of retrieval is an alternative to those in which the index of refraction is held fixed, but particle size is adjusted based on the wavelength dependence of the retrieved optical depths [*Durkee et al.*, 1991; *Higurashi and Nakajima*, 1999; *Mischenko et al.*, 1999].

[4] Optical depths retrieved for the different aerosol models were compared with simultaneous surface-based measurements obtained with various radiometers deployed for INDOEX. The comparisons covered the winter monsoons for 1996–2000.

[5] The retrieved optical depths along with the corresponding aerosol models were used in broadband radiative transfer calculations of the top of the atmosphere and surface aerosol direct radiative forcing under cloud-free conditions. Estimates of the top of the atmosphere forcing were found to be somewhat insensitive to the choice of the aerosol model used to retrieve the aerosol properties. That is, as long as the estimate of the top of the atmosphere radiative forcing is derived based on the same aerosol model used to retrieve the aerosol properties, errors in the estimate of the radiative forcing will be partially compensated by errors in the optical depths retrieved using the same aerosol model. On the other hand, because the different models produce different amounts of absorption in the atmosphere, the radiative forcing at the surface (and that of the atmosphere) is, of course, sensitive to the aerosol model.

[6] While the procedures for estimating the aerosol direct radiative forcing for cloud-free conditions are straightforward, those for determining the forcing under cloudy conditions require simultaneous measurements of the cloud properties. The forcing depends not only on the properties of the aerosol but also on the properties of the clouds and the vertical distribution of both the aerosol and the clouds [*Haywood et al.*, 1997; *Ramanathan et al.*, 2001]. As part of this study, individual AVHRR fields of view were identified as either cloud-free, or overcast by optically thick clouds from a single-layered cloud system. The fields of view that were neither cloud-free nor overcast by optically thick, single-layered clouds were taken to be partly cloud covered. For the clouds encountered during INDOEX, few layered cloud systems met the criteria required for overcast fields of view (<5%), even at the full, 1-km resolution of the AVHRR. In addition, because the criteria used to identify overcast fields of view were limited to identifying optically thick, layered cloud systems, fields of view overcast by thin cirrus, or overcast by clouds distributed in altitude were potentially identified as being partly cloudy. As with other methods for determining cloud properties, the derived properties are a function of the procedures used to identify cloudy scenes and to extract the properties for the clouds. Results for different approaches to determining cloud properties diverge most for scenes in which the cloud elements cannot be resolved by the observing radiometer [*Wielicki and Parker*, 1992], as was common in INDOEX. Because of the range of possible cloud properties, sensitivity studies were performed in which different assumptions concerning the effects of clouds on the aerosol direct radiative forcing were employed to determine the range of the resulting aerosol direct radiative forcing at the top of the atmosphere and the surface.

2. Retrieval of Aerosol Properties

[7] In order to retrieve aerosol properties, reflected sunlight measured with the AVHRR must be compared with

that obtained through radiative transfer calculations. Such comparisons require that the AVHRR observations of reflected sunlight be calibrated. Because there is no onboard calibration source for AVHRR Channels 1 and 2, the extensive ice sheets of Greenland and Antarctica were used to calibrate the observations [*Loeb*, 1997; *Tahnk and Coakley*, 2001a, 2001b].

[8] The reflectances of the cloud-free fields of view were compared with those calculated assuming that the aerosol had a given set of properties. The aerosol optical depth and an index of aerosol type were selected to give the best agreement between observed and calculated reflectances. The selected optical depth and properties were then taken to be the retrieved values. This section briefly describes the method used to identify cloud-free fields of view, the aerosol models along with the radiative transfer model used to calculate the reflectances, and the procedures used to extract aerosol properties by comparing the observed and calculated reflectances.

2.1. Scene Identification

[9] Fields of view were identified as cloud-free if they exhibited locally uniform reflected sunlight and thermal emission on scales of ~8 km (2 × 2 pixel arrays) for the 4-km AVHRR Global Area Coverage (GAC) observations. For cloud-free ocean scenes, the standard deviation of the 0.64-μm (AVHRR Channel 1) reflectance for localized arrays of pixels had to be less than 0.004. The standard deviation of the 11-μm (AVHRR Channel 4) emission had to be less than 0.5 mW m^{-2} sr^{-1} cm, equivalent to ~0.3 K for the brightness temperatures associated with the cloud-free oceans. Away from regions of sun glint, cloud-free ocean scenes were required to have a ratio of the near infrared (0.84 μm, AVHRR Channel 2) reflectance to visible (0.64 μm, AVHRR Channel 1) reflectance that was less than 0.85. Overcast pixels produce values of near unity for this ratio while pixels with vegetated land produce values >1. Here, sunlight was taken to be outside of the sun glint region if the light was reflected at angles greater than 40° from the direction of specular reflection for a flat surface.

[10] Within each ~250-km scale region, the distribution of radiances for pixels that exhibited locally uniform reflection and emission and which also had low near infrared to visible reflectance ratios were used to establish thresholds for visible reflectances and 11-μm emission suitable for the cloud-free ocean pixels. Of the radiances for these pixels, the 95th percentile of the visible reflectance was taken as an upper limit and the 5th percentile of the 11-μm emission was taken as a lower limit for cloud-free pixels. These thresholds were applied to all fields of view that exhibited locally uniform emission and reflection and which had low near infrared to visible reflectance ratios and lay within a 150-km scale subregion centered within the larger ~250-km scale region.

[11] Likewise, fields of view were identified as overcast by a single-layered cloud system if they exhibited locally uniform emission at 11 μm. For overcast pixels, the standard deviation of the 11-μm radiance for the pixel arrays had to be less than 0.5 mW m^{-2} sr^{-1} cm, which for low-level clouds is equivalent to a standard deviation of 0.4 K in brightness temperatures. Pixels that exhibited neither locally uniform reflectances nor locally uniform emitted radiances were presumed to be partly cloud covered. The 50th percentile of the reflectances for the partly cloudy pixels was used as a minimum reflectance for pixels to be identified as overcast by optically thick clouds. This visible threshold was applied to the fields of view exhibiting locally uniform emission that were not cloud-free in order to identify fields of view that were overcast by optically thick, layered cloud systems.

[12] This pixel identification process was repeated region by region and subregion by subregion until all fields of view within the overpass were identified. The regions and subregions were overlapped to ensure that all pixels were identified.

[13] The identification scheme was designed to identify ensembles of pixels that were representative of cloud-free pixels and pixels overcast by optically thick, layered clouds within the ~150 km region being studied. The scheme does not identify all cloud-free fields of view, nor does it identify all overcast fields of view within the region. In particular, cloudy fields of view overcast by a system of clouds residing in multiple cloud layers along with fields of view overcast by thin cirrus are identified as being partly cloud covered. For cloud-free fields of view, the identification scheme specifically avoids individual fields of view that may be surrounded by cloud and are thus likely to be cloud contaminated in favor of fields of views that are contiguous with all pixels exhibiting properties that are typical of cloud-free scenes. As discussed by *Tahnk and Coakley* [2002], about 15% of the 4-km AVHRR GAC fields of view were typically identified as being cloud-free for the Indian Ocean in the Northern Hemisphere. Thus, fields of view suitable for aerosol retrievals were plentiful. The majority of the 4-km fields of view were found to be partly cloudy. Relatively few (<5%) were identified as being overcast by single-layered optically thick clouds and of these, a sizable fraction were associated with upper-level systems. By varying the criteria used to identify cloud-free fields of view, so that the identified fields of view were subjected to greater and lesser levels of cloud contamination, cloud contamination was found to contribute less than 0.05 to the retrieved 0.55-μm aerosol optical depth. Here, 0.55-μm is used as the reference wavelength for reporting aerosol optical depths. This level of cloud contamination is less than half of the average optical depths found for pristine ocean regions of the Southern Hemisphere.

2.2. Aerosol and Radiative Transfer Models

[14] Table 1 lists characteristics of the aerosol models used in the retrievals. The properties are given for a relative humidity of 70%. As mentioned in the introduction, the average continental and tropical marine aerosol models were taken from *Hess et al.* [1998]. These models, along with the FFP model, are multicomponent models. For comparison, retrievals were also performed with the models used in the NOAA Phase 1 and Phase 2 retrieval algorithms [*Stowe et al.*, 1997]; these are single-component models.

[15] Aerosol properties were retrieved by matching observed reflectances for the cloud-free fields of view to those computed for a particular aerosol. The reflectances were calculated using DISORT [*Stamnes et al.*, 1988]. Absorption by O_3, O_2, and H_2O within the AVHRR Channel 1 and 2 passbands was treated using the correlated

Table 1. Properties of Aerosols at 70% Relative Humidity[a]

Component	Number Fraction	Effective Radius, μm	0.55-μm Extinction Efficiency	Ångström Coefficient	0.65-μm Extinction Efficiency	Single-Scattering Albedo	Asymmetry Parameter	0.80-μm Extinction Efficiency	Single-Scattering Albedo	Asymmetry Parameter
					Average Continental					
Water soluble	0.458	0.145	0.842	1.60	0.656	0.977	0.675	0.463	0.964	0.653
Insoluble	2.61×10^{-5}	3.60	2.26	−0.09	2.30	0.750	0.811	2.34	0.776	0.794
Soot	0.542	0.039	0.481	1.41	0.380	0.173	0.302	0.284	0.133	0.263
Composite	*1.0*	*0.205*	*0.825*	*0.69*	*0.655*	*0.899*	*0.678*	*0.638*	*0.903*	*0.682*
					Tropical Marine					
Water soluble	0.983	0.145	0.842	1.60	0.656	0.977	0.675	0.463	0.964	0.653
Sea salt (acc. mode)	0.017	1.324	2.56	−0.08	2.62	1.000	0.781	2.64	1.000	0.785
Sea salt (coarse mode)	2.17×10^{-6}	10.860	2.11	−0.03	2.12	1.000	0.848	2.13	1.000	0.844
Composite	*1.0*	*1.011*	*2.01*	*0.01*	*2.00*	*0.998*	*0.771*	*2.01*	*0.997*	*0.774*
					FFP					
Water soluble	0.202	0.145	0.842	1.60	0.656	0.977	0.675	0.463	0.964	0.653
Sea salt (acc. mode)	1.20×10^{-4}	1.324	2.56	−0.08	2.62	1.000	0.781	2.64	1.000	0.785
Sea salt (coarse mode)	1.11×10^{-6}	10.860	2.11	−0.03	2.12	1.000	0.848	2.13	1.000	0.844
Mineral (transport)	1.83×10^{-5}	1.843	2.36	−0.12	2.41	0.877	0.851	2.47	0.906	0.733
Soot	0.798	0.039	0.481	1.41	0.380	0.173	0.302	0.284	0.133	0.263
Composite	*1.0*	*0.500*	*0.863*	*0.58*	*0.725*	*0.847*	*0.704*	*0.694*	*0.867*	*0.711*
					NOAA Phase 2					
–	1.0	0.349	2.17	0.84	1.92	1.000	0.744	1.58	1.000	0.732
					NOAA Phase 1					
–	1.0	0.085	0.315	1.49	0.246	1.000	0.595	0.180	1.000	0.595

[a]The extinction efficiency is the extinction cross section divided by πR_e^2 where R_e is the effective radius.

k-distributions described by *Kratz* [1995]. The *McClatchey et al.* [1972] tropical climatological profiles of temperature and humidity were used to calculate the reflectances. As discussed in section 4, using midlatitude summer climatological profiles in place of the tropical profiles had little effect on the retrieved optical depths. Following *Rajeev et al.* [2000], the aerosols were uniformly mixed below 1 km and distributed with a scale height of 0.8 km between 1 and 8 km. No aerosol was placed above 8 km. The vertical distribution is consistent with that derived from lidar returns in the INDOEX region as reported by *Satheesh et al.* [1999]. In addition, optical properties of the aerosols were calculated using a relative humidity of 78% for 0–1 km, 62% for 1–2 km, and 35% above 2 km as proposed by *Satheesh et al.* [1999] based on radiosonde data collected at KCO for the February–March, 1998 INDOEX FFP. *Rajeev et al.* [2000] adopted the same profile of relative humidity for retrievals of optical depths using the FFP aerosol model.

[16] Reflectances were calculated for aerosol optical depths at a standard wavelength of 0.55 μm. The optical depths ranged from 0–0.9 in steps of 0.1; the solar zenith angle ranged from 0°–85° in steps of 5°; the cosine of the view zenith angle ranged from 0.3–1.0 in steps of 0.1, and the solar relative azimuth angle ranged from 0°–180° in steps of 10°. The ocean surface was taken to be Lambertian with an albedo of 0.005 at both wavelengths. This value is somewhat elevated from that expected for water surfaces for radiation reflected in the direction of backward scattered sunlight. The slight elevation is meant to account for the small contribution to the reflected light from sun glint-specifically, radiation that is reflected by the ocean surface and then scattered by the atmosphere into the radiometer's field of view. The value chosen for the albedo minimized the average differences between optical depths retrieved at both visible and near infrared wavelengths and those measured at the surface. When comparing with observed reflectances, the calculated reflectances were linearly interpolated to the desired Sun-Earth-satellite geometry.

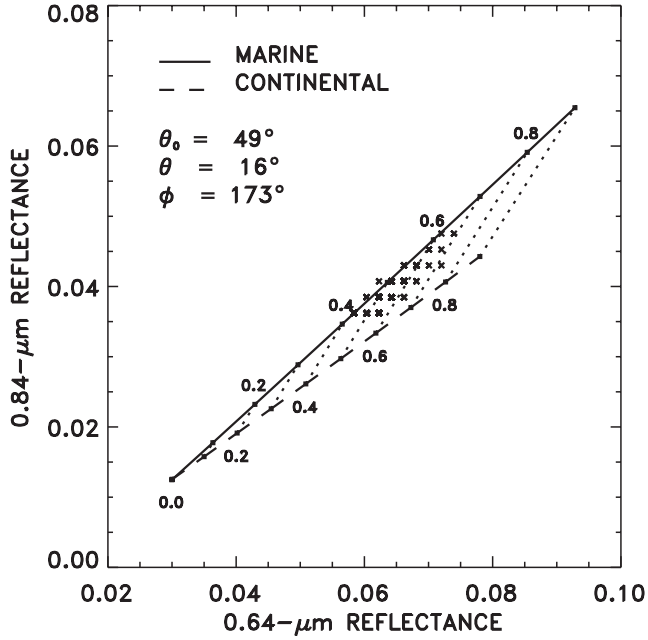

Figure 1. Calculated and observed 0.64 and 0.84-μm reflectances for ~100 km region of the Arabian Sea. Average values are given for the solar zenith, θ_0, satellite zenith, θ, and relative solar azimuth angles, ϕ, of the observations. Observations (×) are from the NOAA-14 AVHRR for a pass during the INDOEX Intensive Field Phase, February 1999. Reflectances are given for the average continental (dashed line) and tropical marine aerosol models of *Hess et al.* [1998]. Dotted lines are lines of constant 0.55-μm optical depth (indicated by the adjacent numbers) for mixtures of the average continental and tropical marine aerosol.

2.3. Aerosol Retrieval Schemes

[17] Three types of retrievals were used. In the simplest scheme, reflectances were calculated for a single aerosol model and then optical depths were retrieved by seeking agreement between calculated and observed reflectances at one wavelength, for example, the 0.64-μm Channel 1 of AVHRR [*Stowe et al.*, 1997; *Rajeev et al.*, 2000].

[18] In the second, the new scheme developed for this study, two aerosol models were used and reflectances were calculated for the visible and near infrared wavelength channels of the AVHRR. The retrieved optical depth and the fraction of each aerosol type contributing to the retrieved optical depth were selected so that the observed visible and near infrared reflectances agreed with the calculated values as illustrated in Figure 1. The reflectances in the figure are the isotropic reflectances given by

$$r(\theta_0, \theta, \phi) = \frac{\pi I}{\mu_0 F}$$

where I is the radiance as measured by the radiometer; F is the value of the solar constant appropriate for the spectral channel of the radiometer and the time of year, and μ_0 is the cosine of the solar zenith angle. The reflectances at the two wavelengths were calculated for the viewing geometry associated with the observation as given by the solar zenith angle, θ_0, the satellite zenith angle, θ, and the solar relative azimuth angle, ϕ. Aerosol properties at 0.65 μm were used in calculations of the reflectances for AVHRR Channel 1 at 0.64 μm, and properties at 0.80 μm were used in calculations of the reflectances for AVHRR Channel 2 at 0.84 μm.

[19] Figure 1 shows the cloud-free reflectances for the individual models, the tropical marine aerosol (solid line) and the average continental aerosol (dashed line). For the range of optical depths considered in this study, the reflectances are almost linearly proportional to the optical depths even for sizable aerosol burdens. As a result, the reflectances at any two wavelengths are almost linearly related. The figure shows that even for 0.55-μm optical depths as large as 0.9, departures of the reflectances from a linear relationship are small. Consequently, a natural rendition of the reflectances would be as a mixture of the reflectances contributed by each component. To the extent that the reflectances are linear in optical depth, this treatment is equivalent to taking the aerosol to be a mixture of the optical depths of the two aerosol components, which in turn, is equivalent to taking the aerosol to be a mixture of number

concentrations. The dotted lines joining the lines associated with the individual models are thus lines of constant optical depths for various aerosol mixtures. The combined reflectance is then given by

$$r_i(\tau) = f r_{iC}(\tau) + (1-f) r_{iM}(\tau) \quad (1)$$

where $r_i(\tau)$ is the cloud-free ocean reflectance in AVHRR channel $i = 1, 2$ when the optical depth of the mixed aerosol is τ at the standard wavelength; $r_{iC}(\tau)$ is the channel i reflectance for the cloud-free ocean over which an average continental aerosol has optical depth τ at the standard wavelength; $r_{iM}(\tau)$ is the corresponding reflectance for the tropical marine aerosol; f is the fraction of the mixture that is taken to be the average continental aerosol, and $1-f$ is the fraction of the mixture that is taken to be the tropical marine aerosol. As defined, f plays the role of a mixing fraction as commonly used to describe the thermodynamic properties of air parcels that undergo mixing. In this case, for $f = 1$, the aerosol is the average continental aerosol; for $f = 0$, the aerosol is the tropical marine aerosol. Because the slopes of the Channel 2 to Channel 1 reflectances are numerically rather similar for the average continental and the tropical marine aerosols, which, of course, is unfortunate for the design of a retrieval scheme, the slope of the Channel 2 to Channel 1 reflectances is approximately given by

$$\frac{r_1(\tau) - r_{10}}{r_2(\tau) - r_{20}} \cong f\left(\frac{r_{1C}(\tau) - r_{10}}{r_{2C}(\tau) - r_{20}}\right) + (1-f)\left(\frac{r_{1M}(\tau) - r_{10}}{r_{2M}(\tau) - r_{20}}\right), \quad (2)$$

where r_{i0} is the ocean reflectance under cloud-free and aerosol-free conditions for channel i. In addition, since the reflectances are almost linearly related for the range of optical depths being considered, (2) is approximately equivalent to

$$\frac{r_1(\tau) - r_{10}}{r_2(\tau) - r_{20}} \cong f\left(\frac{r_{1C}(\tau_0) - r_{10}}{r_{2C}(\tau_0) - r_{20}}\right) + (1-f)\left(\frac{r_{1M}(\tau_0) - r_{10}}{r_{2M}(\tau_0) - r_{20}}\right) \quad (3)$$

with τ_0 a reference optical depth at the standard wavelength. Here $\tau_0 = 0.9$. For each cloud-free pixel, f is derived from (3). In other words, the aerosol mixing fraction, f, is derived from the slope of the Channel 1 to Channel 2 reflectance departures from the values expected for cloud-free and aerosol-free conditions. Once f is determined, the optical depth at the standard wavelength is derived from the reflectances themselves, as given by (1).

[20] Discrepancies between values of the slopes calculated using (1) separately for Channels 1 and 2 and those obtained using (3) arise because the reflectances are, in fact, nonlinear functions of the optical depths. For the range of 0.55-μm optical depths considered here ($0.1 \leq \tau \leq 0.9$), the nonlinearity is relatively weak as long as the solar zenith and satellite zenith angles are less than 65° and the 0.55-μm optical depth is less than 0.9. Of the data analyzed, few retrievals were encountered with such large satellite and solar zenith angles and such large optical depths. Simulations were performed in which reflectances were calculated using (1) and f was derived using (3). In the simulations, the range of viewing geometries used in the retrievals was explored, with the exception that the solar zenith and satellite zenith angles were limited to being less than 65°. The results of the simulations indicated that the nonlinearity of the reflectances biased f slightly toward 1. The retrievals favored the average continental aerosol. The retrieved values of f had a bias of 0.06 and an RMS difference about the bias of 0.1. The retrieved values of τ had a negligible bias with an RMS difference of 0.01. Of course, the nonlinearity of the reflectances could be accounted for in the retrievals by, for example, iterating the solutions for f and τ until suitable convergence criteria were met. The scheme described here, however, was adopted because it was simple and produced results that were reasonably accurate.

[21] To illustrate the relationship between f, τ, and the reflectances, the symbols (×) in Figure 1 represent the reflectances from the NOAA-14 AVHRR for the cloud-free pixels found within a 100-km scale portion of the Arabian Sea during INDOEX. Each point is now interpreted as being due to a specific mixture of the two aerosols and the mixture produces a specific optical depth at the standard wavelength, as indicated in the figure. The discrete values of the observed reflectances are due to changes at the single count level for the AVHRR.

[22] The average continental and tropical marine aerosol models, described by *Hess et al.* [1998], were chosen for this retrieval scheme with the following considerations. First, the aerosol over the Indian Ocean was expected to be a mixture of a continental haze with absorbing aerosols, as is the case for the average continental model. Second, the aerosol was also expected to have a prominent marine component, particularly when levels of pollution from the continent were low. Third, the average continental and tropical marine aerosol models serve as standard models and using these models in the retrieval scheme allows an assessment of their utility in estimating aerosol burdens and the direct aerosol radiative forcing. Fourth, of the aerosol models described by *Hess et al.* [1998], the average continental and tropical marine aerosols, for most viewing geometries, spanned the largest portion of the two-channel reflectance domain like that shown in Figure 1. In other words, the curves in Figure 1 produced individually by these two aerosol models have the largest possible separation. The slopes of these curves are governed primarily by the size of the particles responsible for scattering. In the case of the tropical marine aerosol, the particle sizes are relatively large, effective radius ~1.0 μm (Table 1), and for the average continental aerosol the particle sizes are relatively small, effective radius ~0.2 μm. Increasing the amount of sunlight absorbed by these aerosols, by adding soot as an additional component to each, has little effect on the slopes of the reflectance curves. The additional absorption simply diminishes the reflectances produced by a given optical depth thereby leading to higher retrieved optical depths for a given set of reflectances. The NOAA Phase 1 model has smaller particle sizes, and would produce a larger 2-channel reflectance domain when combined with the tropical marine aerosol. This model was not adopted here, however, because the effective radius ~0.08 μm is well below those found in the INDOEX region [*Satheesh et al.*, 1999; *Clarke et al.*, 2002; *Quinn et al.*, 2002]. For the viewing geometries encountered in INDOEX, the NOAA Phase 2 model produces a slope for the two-channel reflectances that is nearly identical to that of the average continental aerosol, and for most viewing geometries, the FFP

model produces a slope similar to that of the tropical marine aerosol, but for some viewing geometries the slope of the reflectances for the FFP model slightly exceeds that of the tropical marine aerosol.

[23] For simplicity, the retrieval scheme just described will be referred to as the 2-channel, 2-model scheme. To complete this retrieval scheme, rules were prescribed for dealing with reflectances that lay outside the domain bracketed by the reflectances associated with mixtures of the two aerosol models. For reflectances outside the bracketed domain, the retrieved aerosol type was set to the model which had reflectances nearest those observed, either the average continental or the tropical marine aerosol model, and the optical depth was taken to be that which produced the smallest RMS differences between the observed and calculated reflectances for both channels. Because it uses reflectances at two wavelengths in a least squares solution, this procedure differs from that typically employed in single-channel, single-aerosol model retrieval schemes. This 2-channel, single-model scheme is the third retrieval scheme considered here. Sections 4 and 5 explore differences between the results obtained with the different retrieval schemes.

[24] Interestingly, even though the tropical marine and average continental aerosols bracket the domain of possible reflectances for the two AVHRR channels, a substantial number of observations fell outside of the bracketed domain. In the Southern Hemisphere, for the 8-day sample of data described in section 5, 40% of the reflectances fell within the domain of the two models, 40% fell to the side of the continental aerosol, and 20% fell to the side of the tropical marine aerosol. For the Northern Hemisphere, the percentages were 55% within the domain, 29% on the side of the continental aerosol, and 16% on the side of the marine aerosol. The large fraction of reflectances falling outside the domain is viewed as unsatisfactory. Reflectances that fall to the side of the average continental model may be caused by the nonlinear relationship between the reflectances not being accounted for in the retrievals, but it may also suggest that the particles reflecting the sunlight are smaller than those in the average continental model. The reflectances that fall to the side of the tropical marine aerosol may suggest cloud contamination, either by small amounts of low-level clouds or by thin cirrus. The slope of the reflectances for the tropical marine aerosol is close to that for clouds. Of course, reflectances may fall outside the expected domain because of errors in the calibration of the AVHRR, errors in the model used to calculate the reflected light contributed by the underlying ocean, and errors in accounting for absorption by atmospheric gases. Reducing the number of cloud-free ocean scenes with reflectances that fall outside those expected remains a challenge.

3. Radiative Forcing

[25] Once the mixing fraction and optical depth of the aerosol mixture was obtained, the diurnally averaged broadband, 0.2–4.0-μm, net radiative flux at the top of the atmosphere and surface were calculated. For cloud-free pixels, the diurnally averaged broadband radiative fluxes are given by

$$F = fF_C(\tau) + (1-f)F_M(\tau). \quad (4)$$

where, as in (1), f is the fraction of the mixture determined to be the average continental aerosol; $F_C(\tau)$ is the diurnally averaged radiative flux associated with the average continental aerosol for the optical depth at the standard wavelength, τ, and $F_M(\tau)$ is the corresponding flux for the tropical marine aerosol. The form of (4) for the radiative fluxes is justified because the fluxes for the cloud-free atmosphere are nearly linear with optical depth for the range of 0.55-μm optical depths (0.1–0.9) being considered. The diurnally averaged quantities were derived for each 0.1 increment in the 0.55-μm optical depth ($0.1 \leq \tau \leq 0.9$) for the solar zenith angles associated with a particular latitude zone on the day of observation. Fluxes were then linearly interpolated to the optical depth retrieved for each observation.

[26] For the broadband radiative fluxes, the solar spectrum was divided into 13 spectral intervals: 12 intervals of approximately equal widths were distributed between 0.2 and 0.9 μm and one interval covered 0.9–4.0 μm and was used to account for absorption by water vapor as described by *Lacis and Hansen* [1974]. Scattering and absorption by aerosols in the 0.9–4.0-μm band were calculated using optical properties at 1.0 μm. Optical depths for Rayleigh scattering were taken to be given by

$$\tau_{R\lambda} = \tau_{R0}\left(\frac{\lambda_0}{\lambda}\right)^4$$

with $\tau R_0 = 0.098$, the Rayleigh optical depth at $\lambda_0 = 0.55$ μm. The Rayleigh optical depths are consistent with the those given by *Pendorf* [1957]. Rayleigh optical depths were set to zero for wavelengths greater than 0.9 μm. Absorption cross sections for ozone were taken from data given by *Houghton* [1989]. Absorption calculated using these cross sections agrees with the absorption calculated using the *Lacis and Hansen* [1974] parameterization. For these broadband fluxes the ocean albedo was taken to be Lambertian and the value was set to the planar albedo obtained from *Cox and Munk* [1954] for a surface wind speed of 5 m sec^{-1}. The ocean albedo is almost independent of wavelength and the spherical albedo is 0.06. Note, this value differs from the value of 0.005 used in the retrieval of optical depths. For estimates of radiative fluxes, account is made for light reflected not only in the direction of backscattered sunlight, as is the case for the retrieval of the optical depths, but in all directions, including light reflected for angles affected by sun glint.

[27] The aerosol direct radiative forcing was calculated for each 1° × 1° latitude-longitude region. For regions that contained cloud-free pixels and for which no upper-level clouds were evident, the optical depth and aerosol mixing fraction derived for the cloud-free pixels were used to derive the diurnally averaged broadband fluxes for both the cloud-free portions of the region and the portions overcast by low-level clouds. Regions were taken to contain only low-level clouds provided the 5th percentile of the 11-μm emission for the pixels in the region satisfied $I_{5th} > I_C$ with $I_C = 75$ mW m^{-2} sr^{-1} cm, which is equivalent to a brightness temperature of 275 K and to the emission with opaque clouds at an altitude of 4 km in the tropics. I_C was chosen to be well below the mode of the 11-μm emission associated with pixels overcast by the low-level, layered clouds encountered in INDOEX.

[28] For regions with only low-level clouds, the average radiative forcing was taken to be given by

$$F = \frac{[n_S + (1 - A_{CP})n_P]F_S + (A_{CP}n_P + n_O)F_O}{n} \quad (5)$$

where F_S is the radiative flux for the cloud-free pixels; n_S is the number of cloud-free pixels; A_{CP} is the average fraction of the partly cloudy pixels that is overcast; n_P is the number of partly cloudy pixels; n_O is the number of pixels overcast by optically thick, layered clouds; F_O is the flux associated with the overcast pixels, and n is the total number of pixels in the region. To determine A_{CP}, reflectances at 0.64 μm were taken to be given by the analogous relationship,

$$r = \frac{n_S r_S + (A_{CP}n_P + n_O)r_O}{n} \quad (6)$$

where r_S is the average reflectance associated with cloud-free pixels and r_O is the average reflectance associated with pixels overcast by optically thick, layered clouds. As noted in section 5, $r_O = 0.44$ and $A_{CP} = 0.48$ are suitable average values for low-level clouds in the INDOEX region. For the range of viewing geometries used in the retrievals, the reflectance for overcast pixels is consistent with a visible optical depth of 8. In the evaluation of the aerosol direct radiative forcing for overcast regions, a homogeneous cloud layer between 1 and 2 km with a visible optical depth of 8 was imbedded in the haze.

[29] For the period being analyzed, cloud-free pixels in each 1° × 1° latitude-longitude region were used to derive an average mixing fraction, optical depth, top of the atmosphere and surface net solar radiative fluxes for cloud-free conditions. For regions that contained no cloud-free pixels on a particular satellite pass, these average cloud-free radiative fluxes were used to determine the radiative fluxes for the portions of the region estimated to be cloud-free at the time of observation. The average optical depth and aerosol mixing parameter were used to obtain the radiative fluxes for the portions of the region overcast by low-level, layered clouds.

[30] Regions were taken to be overcast by upper-level clouds when the average 11-μm emission fell below I_C and the 0.64-μm reflectance was greater than r_O. The aerosol direct radiative forcing was set to zero for these regions. The top of the atmosphere and surface solar radiative fluxes are relatively insensitive to aerosol optical depths when an aerosol lies beneath optically thick clouds. Two different approaches were used for regions that were not overcast by upper-level clouds but which, based on the 5th percentile of the 11-μm emission, contained upper-level clouds. In the first, the direct radiative forcing was set to zero for all 1° × 1° latitude-longitude regions that showed evidence of upper-level clouds. In the second, regions containing upper-level clouds were not included in the analysis. Instead, the radiative forcing for a particular geographic region was set to the average forcing obtained when no upper-level clouds were present. The effect of the latter approximation is to overestimate the direct radiative forcing due to the aerosol. Some of the upper-level clouds are bound to attenuate the effect of the aerosols on the top of the atmosphere and surface radiative fluxes. On the other hand, setting the radiative forcing to zero for all upper-level clouds leads to an underestimation of the direct radiative forcing due to aerosols. Thin cirrus and upper-level clouds that cover only a portion of a 1° × 1° latitude-longitude box will not fully attenuate the effect of the aerosol. Presumably, the average radiative forcing due to the aerosol falls between these two limiting cases. Finally, as discussed in section 5, estimates of the top of the atmosphere and surface aerosol direct radiative forcing were made in which the forcing was also set to zero for portions of regions overcast by low-level layered clouds.

4. Comparison of Retrieved Optical Depths and Surface Measurements

[31] The optical depths retrieved using the various schemes were compared with surface measurements. At KCO, NASA's Aerosol Robotic Network (AERONET) [*Holben et al.*, 1998] maintained a CIMEL radiometer for which observations began in February 1998. *Jayaraman et al.* [2001] made shipboard measurements from the Indian RV *Sagar Kanya* beginning with cruises in 1996. During the February–March 1999 Intensive Field Phase (IFP), aerosol optical depth measurements were also made from the NOAA R/V *Ron Brown* [*Quinn et al.*, 2002] and the INDOEX operations center on Hulule. Figure 2 shows comparisons of retrieved aerosol optical depths for the 2-channel, 2-model retrieval scheme described in section 2, and single-channel, single-model schemes using the FFP model, and the NOAA-Phase 1 and Phase 2 aerosol models. Surface and satellite observations were compared if they were within one hour of each other and the satellite observations yielded at least 12 cloud-free pixels suitable for aerosol retrievals within 30 km of the surface measurements. All matchups which satisfied these conditions are shown in Figure 2. The error bars in the figure give the standard deviation of the retrieved optical depths for all pixels satisfying the matchup criteria and the standard deviation of the optical depths measured at the surface for the hour before and after the satellite overpass. Here, the surface observations at 0.67 μm were compared with retrieved optical depths at 0.65 μm. The retrieved optical depth was derived from the optical depth at the reference wavelength (0.55 μm) using the size distribution and the optical properties of the various components listed in Table 1. No corrections were applied to account for the effects of the small shift in wavelength between 0.65 and 0.67 μm. For the FFP model, the bias (0.055) and the RMS difference (0.070) are somewhat larger than those reported earlier (0.01 and 0.036, respectively) by *Rajeev et al.* [2000]. The differences are attributed to (1) the use of data for 1996–2000 in these comparisons as opposed to data for 1998 in the earlier study; (2) the use of a different cloud-screening algorithm; (3) the use of different criteria for selecting observations for comparison, and (4) different ocean reflectances used in the retrievals. The current cloud screening and matchup criteria allow more points to be included in the comparison and thus account for the larger RMS difference. *Rajeev et al.* [2000] allowed for effects due to sun glint and to white caps for radiation reflected into the direction of backscattered sunlight. Here a simple Lambertian reflectance of 0.005 was invoked. The larger bias

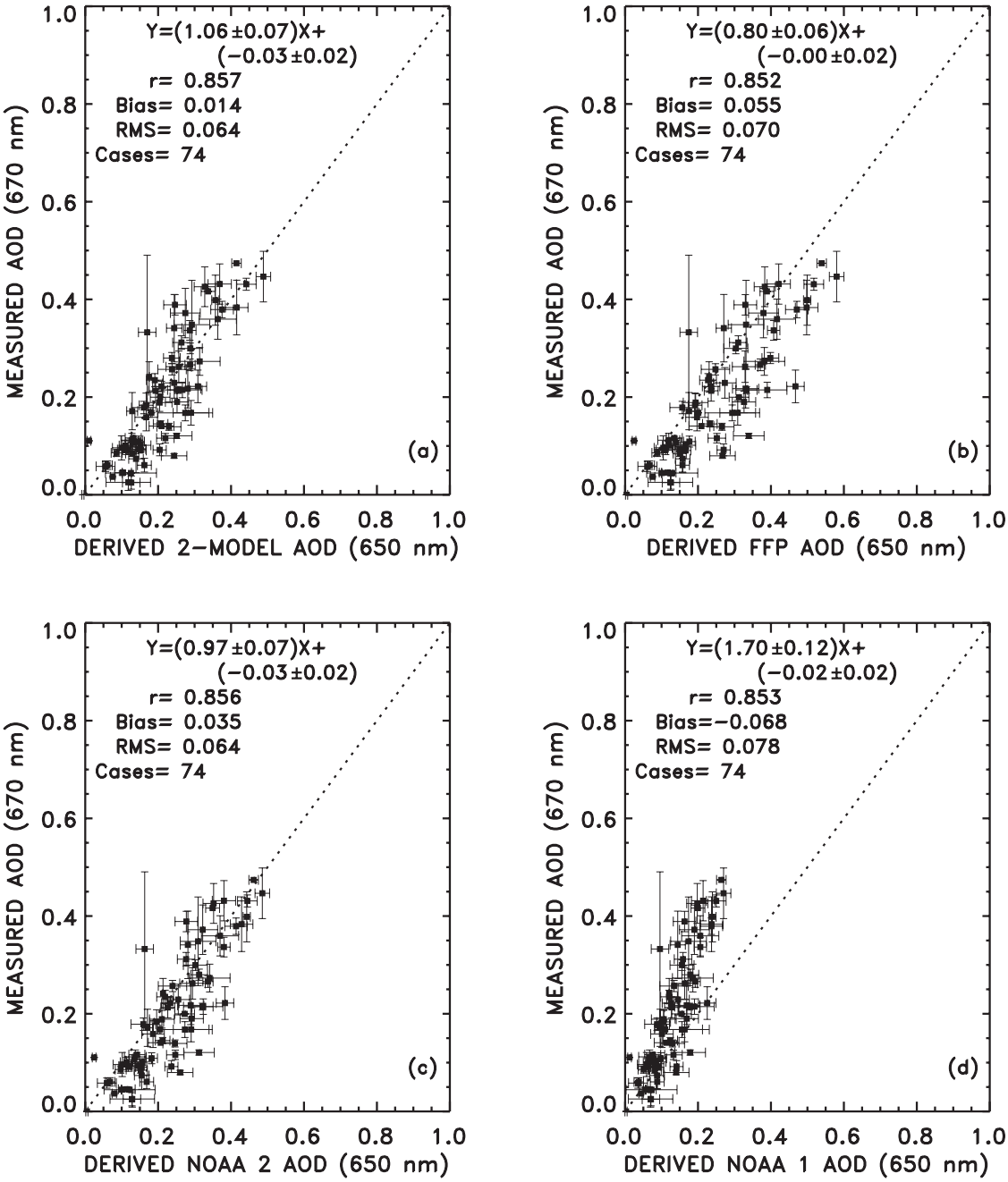

Figure 2. 0.67-μm optical depths measured by surface and shipboard Sun photometers and 0.65-μm optical depths retrieved using (a) the 2-channel, 2-model retrieval; (b) the FFP model; (c) the NOAA Phase 2 model; and (d) the NOAA Phase 1 model. The FFP and NOAA retrievals are all single-channel retrievals. Error bars for the retrieved optical depths give the standard deviation for the fields of view that were within ±30 km of the surface measurements. Error bars for the surface measurements give the standard deviation of the optical depths for ±1 hr surrounding the satellite overpass. Coefficients and estimates of their standard deviations for linear least squares fits are also given.

obtained here for the FFP model may be due to the differences in ocean reflectance.

[32] The results in Figure 2 demonstrate that for all models, the retrieved optical depths were highly correlated with the optical depths measured at the surface. Furthermore, with the exception of the NOAA Phase 1 model, the various aerosol models and retrieval schemes yielded average differences with the surface measurements that were considerably smaller than the RMS differences. Also, the RMS differences were similar for all models. In other words, the NOAA Phase 1 model aside, no aerosol model or retrieval scheme provided significantly better agreement with the surface measurements of optical depths than the others. The shortcomings of the NOAA Phase 1 model were recognized earlier and motivated the switch to the Phase 2 model [*Stowe et al.*, 1997].

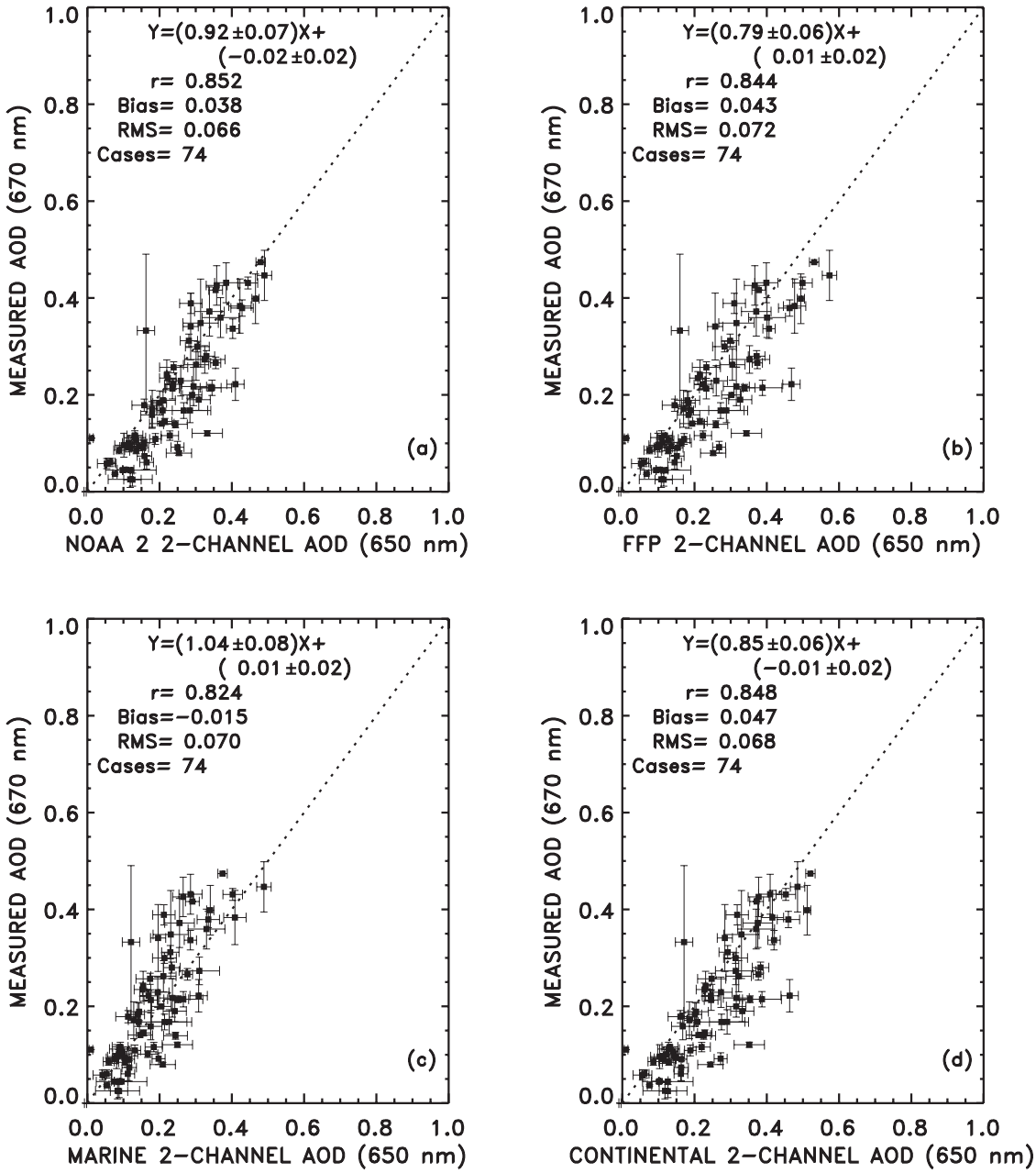

Figure 3. Same as Figure 2 except that all retrievals are single aerosol model, 2-channel retrievals as described in Section 2. Results are for (a) the NOAA Phase 2 model; (b) the FFP model; (c) the tropical marine aerosol model; and (d) the average continental aerosol model.

[33] As described in section 2, the retrieval of aerosol properties reduced to a 2-channel, single-model retrieval scheme in which the RMS difference between observed and calculated 0.64 and 0.84-μm reflectances was minimized when the slope of the 0.84 to 0.64-μm reflectance relationship shown in Figure 1 fell outside the range of values expected for the average continental and tropical marine aerosol models. Figure 3 compares the surface measurements to this two-channel, single aerosol model retrieval scheme for the NOAA Phase 2, the FFP, the tropical marine, and the average continental aerosol models taken separately. For the NOAA Phase 2 and the FFP model, differences with the single-channel retrieval scheme are revealed through comparison of the results in Figure 2b with 3b and Figure 2c with 3a. In all cases, the biases are relatively small compared with the RMS differences about the mean difference. These results indicate that the reflectances at the two wavelengths measured by the AVHRR provide little additional constraint on aerosol properties. This finding may appear to contradict earlier work [*Durkee et al.*, 1991; *Higurashi and Nakajima*, 1999; *Mischenko et al.*, 1999]. In the earlier studies, however, differences in aerosol size indices were obtained only after compositing hundreds of retrievals in order to produce regional scale, monthly mean aerosol properties from daily observations. The 74 cases used here, even though they represent all possible matchups,

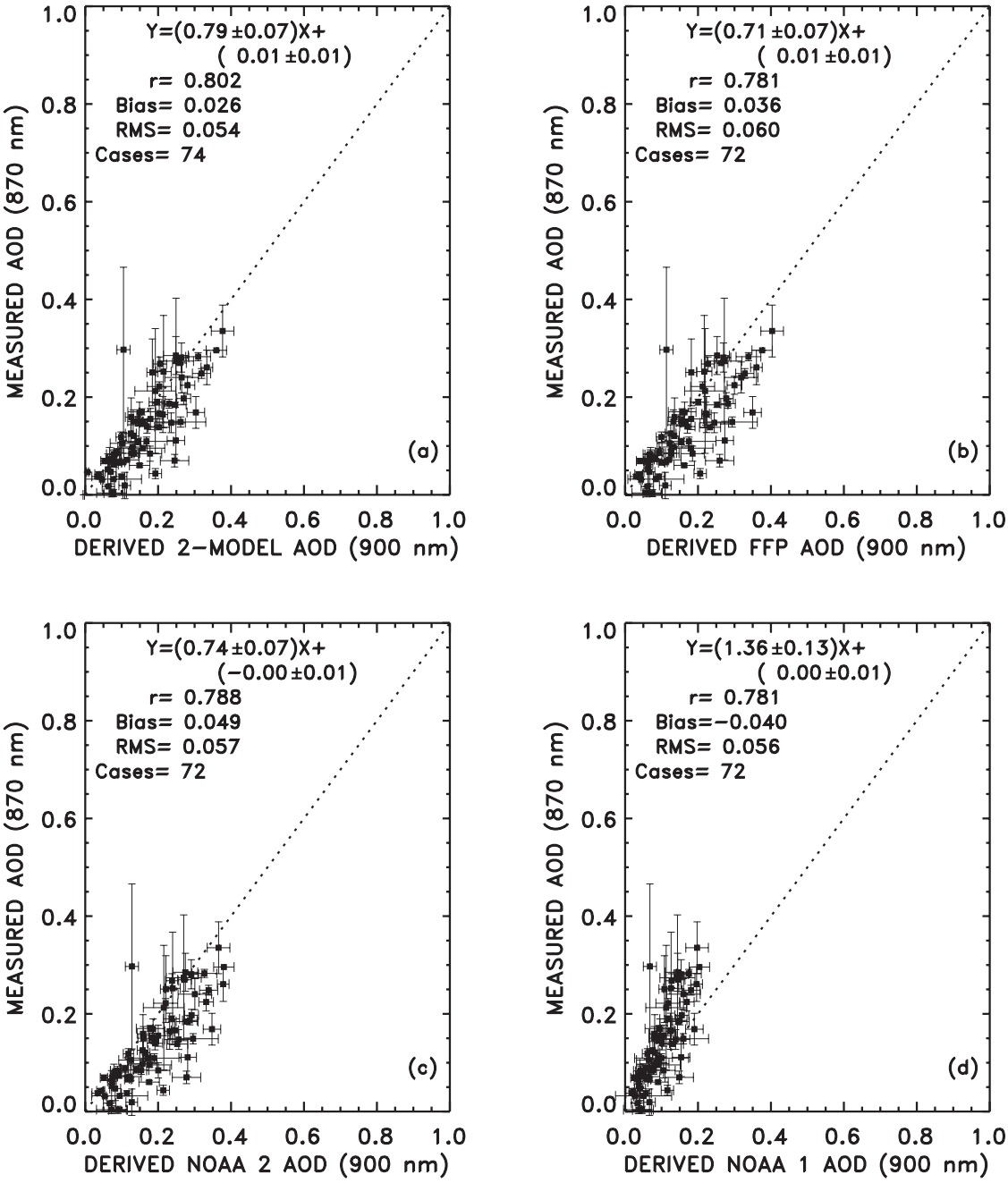

Figure 4. Same as Figure 2 except for surface measurements at 0.87 μm and retrieved optical depths at 0.90 μm.

were evidently too few to discover any benefits gained through using observations at the two wavelengths.

[34] Figure 4 compares the optical depths retrieved at 0.90-μm with values measured at the surface at 0.87 μm. As with the comparisons at visible wavelengths, no attempt was made to account for the small shift in wavelengths between the retrieved and measured optical depths. For the NOAA Phase 1 and Phase 2 models and for the FFP model, the 0.90-μm optical depths were obtained following the same procedures used to derive the 0.65-μm optical depths but with the Channel 2 (0.84 μm) reflectances replacing the Channel 1 (0.64 μm) reflectances for both the observed and calculated reflectances. For the 2-channel, 2-model retrieval scheme, the retrieved 0.90-μm optical depth was derived from the fractions retrieved for the two aerosol components and the optical depth at the standard wavelength retrieved for the aerosol mixture. The figure shows that the agreement at 0.90 μm was similar to that at 0.65 μm although the correlation between the satellite derived and surface-measured optical depths was somewhat weaker.

[35] Instead of comparing optical depths, however, the value of the observations at two distinct wavelengths is better demonstrated by comparing the ratio of the retrieved optical depths at the two wavelengths with the corresponding ratio for the surface measurements, as is done in Figure 5. The dotted lines in the figure indicate the ratio

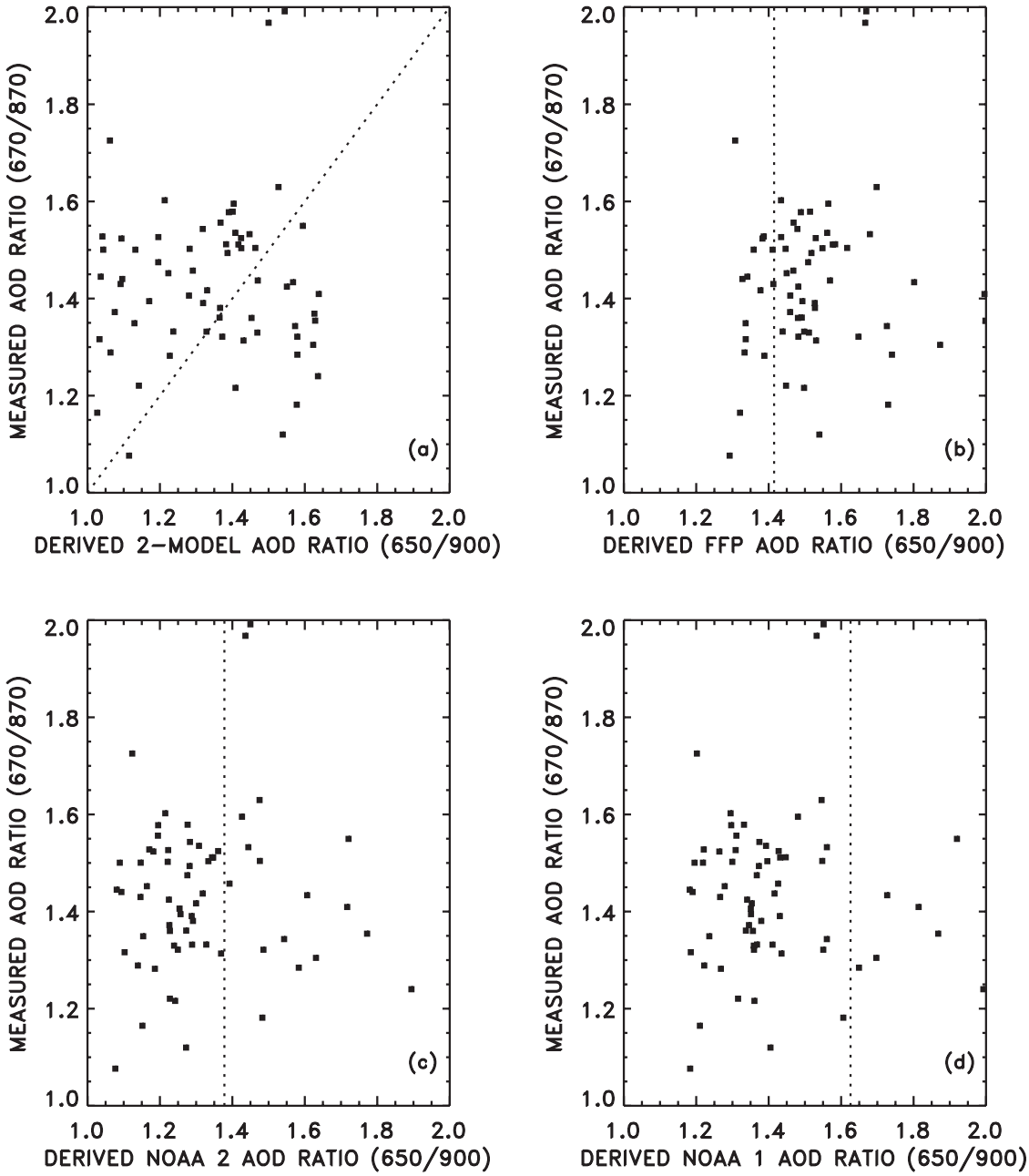

Figure 5. Ratios of optical depths at 0.67 and 0.87 μm for surface measurements and at 0.65 and 0.90 μm for optical depths retrieved from the NOAA-14 AVHRR, for (a) the 2-channel, 2-model scheme; (b) the FFP model; (c) the NOAA Phase 2 model; and (d) the NOAA Phase 1 model. Dotted lines indicate the ratios that would have been obtained had the processes that gave rise to the radiances been properly modeled in the retrieval schemes.

of the optical depths that should have been obtained if the retrievals accurately represented the physical processes that gave rise to the observed reflectances. The scatter of results away from the lines reflects the inadequacies in the retrievals. Such inadequacies are common to all retrieval schemes, regardless of which aerosol model is being used.

[36] Because reflectances at 0.84 μm are affected by water vapor and those at 0.64 μm by ozone, optical depths and 0.84 to 0.64-μm optical depth ratios were derived using midlatitude profiles of water vapor and ozone instead of the tropical profiles. For the 2-channel, 2-model retrieval, the change in the profiles caused a change in optical depth of 0.028 at 0.65 μm and 0.002 at 0.90 μm. These changes had no perceptible effect on the appearance of the optical depth ratios shown in Figure 5a.

5. Evaluation of Aerosol Direct Radiative Forcing

[37] The sensitivity of the top of the atmosphere and surface net solar radiative fluxes to changes in aerosol concentrations is presented in Table 2 for the NOAA Phase 1, NOAA Phase 2, FFP, average continental, and

Table 2. Radiative Forcing Sensitivity[a]

Aerosol Model	$dF/d\tau$, W m^{-2} Unit Optical Depth^{-1}	
	Top of Atmosphere	Surface
	Cloud-Free	
NOAA phase 1	−52	−54
NOAA phase 2	−36	−38
FFP	−21	−92
Tropical marine	−34	−38
Average continental	−27	−75
	Overcast	
Tropical marine	−6	−17
Average continental	+8	−39

[a]Values are calculated for a 0.55-μm aerosol optical depth of 0.3.

tropical marine aerosols for cloud-free conditions. The results are for diurnally averaged shortwave radiative fluxes for 5°N on 1 March, conditions appropriate for INDOEX. The sensitivities are normalized to unit 0.55-μm optical depth, but they are evaluated for an optical depth of 0.3, which is typical of the average conditions for the Arabian Sea and Bay of Bengal found during the February–March 1999 INDOEX IFP. Even though the radiative fluxes are almost linear functions of the aerosol optical depth for the range of optical depths incorporated in this study, the slight nonlinearity causes the sensitivities to decrease with increasing optical depths. The sensitivities for the top of the atmosphere fluxes decrease by approximately 15% for optical depths ranging from 0.2–0.7 for nonabsorbing aerosols, like the NOAA Phase 1 and Phase 2 aerosol models, and by about 35% for the absorbing aerosol models, the average continental and FFP models. The sensitivities for the surface fluxes decreases by about 15% for the same range of optical depths for both absorbing and nonabsorbing aerosols. Through their dependence on the diurnal variation of solar zenith angle at a particular latitude zone for a given day, the sensitivities also vary over the region, but for a given day, the variation is approximately 10% from 30°S–30°N for both top of the atmosphere and surface fluxes.

[38] Table 2 also gives sensitivities of the top of the atmosphere and surface net solar radiative fluxes to changes in optical depths for regions overcast by low-level clouds. Results are presented for the tropical marine and average continental aerosols. As for the cloud-free cases, the column 0.55-μm optical depth of the aerosols is 0.3. As discussed in the previous section, these results were obtained for a homogeneous cloud layer between 1 and 2 km with a visible optical depth of 8 imbedded in haze. For cloud-free conditions, the net solar radiative fluxes at the top of the atmosphere and at the surface decrease with increasing aerosol burden. When low-level clouds are imbedded in an average continental aerosol and the clouds achieve overcast conditions, the absorption of sunlight by the aerosol is sufficient to reduce the albedo of the Earth-atmosphere system compared with its value for similarly overcast but aerosol-free conditions. Consequently, under such conditions, the net solar radiative flux at the top of the atmosphere increases with increasing aerosol burden. Unlike the sensitivities for cloud-free conditions, for overcast conditions, the sensitivity of the top of the atmosphere fluxes to optical depth change is relatively insensitive to the aerosol optical depth provided that the cloud is optically thick, as is the case here. On the other hand, as for cloud-free conditions, the sensitivity of the surface fluxes decreases by about 15% as the aerosol optical depth increases from 0.2–0.7.

[39] For cloud-free conditions, the results illustrate the wide range of the aerosol direct radiative forcing possible for different aerosols. The radiative forcing is a function of aerosol particle size and the extent to which the aerosol absorbs sunlight. At the top of the atmosphere, the radiative flux is least sensitive, per unit optical depth, to the FFP model, for which the sensitivity is −21 W m^{-2} per unit 0.55-μm optical depth, and most sensitive to the NOAA Phase 1 aerosol, for which the sensitivity is −52 W m^{-2} per unit 0.55-μm optical depth. As indicated in Table 1, the differences arise from the relatively strong absorption and relatively large particles in the FFP model, compared with the lack of absorption and relatively small particles in the NOAA Phase 1 model.

[40] Estimates of the top of the atmosphere radiative forcing based on the different aerosol models are, however, in better agreement than the different sensitivities of the reflected fluxes to optical depths would suggest. For example, the large sensitivity obtained for the NOAA Phase 1 model is compensated somewhat by the smaller optical depths retrieved using that model. The effects of such compensation are illustrated in Figure 6 which shows the top of the atmosphere aerosol direct radiative forcing under cloud-free conditions derived for the same cases that were used to compare retrieved and surface measurements of aerosol optical depth. In Figure 6, the radiative forcing derived for the NOAA Phase 1, NOAA Phase 2, and the FFP models are compared with that derived using the 2-channel, 2-model scheme described in section 2. Also, for comparison, Figure 6d shows the direct radiative forcing for the FFP and average continental aerosol models based on the optical depths retrieved using only Channel 1 (0.64-μm) reflectances. As indicated by the single scattering albedos and asymmetry parameters listed in Table 1, the average continental and FFP models have similar scattering properties. The FFP model absorbs more sunlight and thus produces somewhat less forcing at the top of the atmosphere than does the average continental model. Differences in the top of the atmosphere radiative forcing between the 2-channel, 2-model scheme and the other models is smallest for the FFP model. For the 2-channel, 2-model scheme the average radiative forcing is 6.8 W m^{-2}. The average difference with the FFP model is less than 10%.

[41] Figure 7 gives averages of the cloud-free aerosol direct radiative forcing calculated for an 8-day sample of NOAA-14 passes over the INDOEX region drawn from February and March 1999. The radiative forcing is for the top of the atmosphere (TOA), surface (SFC), and the atmosphere (ATM). The values in the parentheses are the standard deviation of the daily averages for the region and reflect the day-to-day variability in the regional means. The results show the differences obtained using the different aerosol models and retrieval schemes. The forcing represents the diurnally averaged, cloud-free radiative forcing for the Arabian Sea, the Bay of Bengal, and the Indian Ocean in the Southern Hemisphere. Consistent with the results in Figure 6, relative differences in the top of the atmosphere

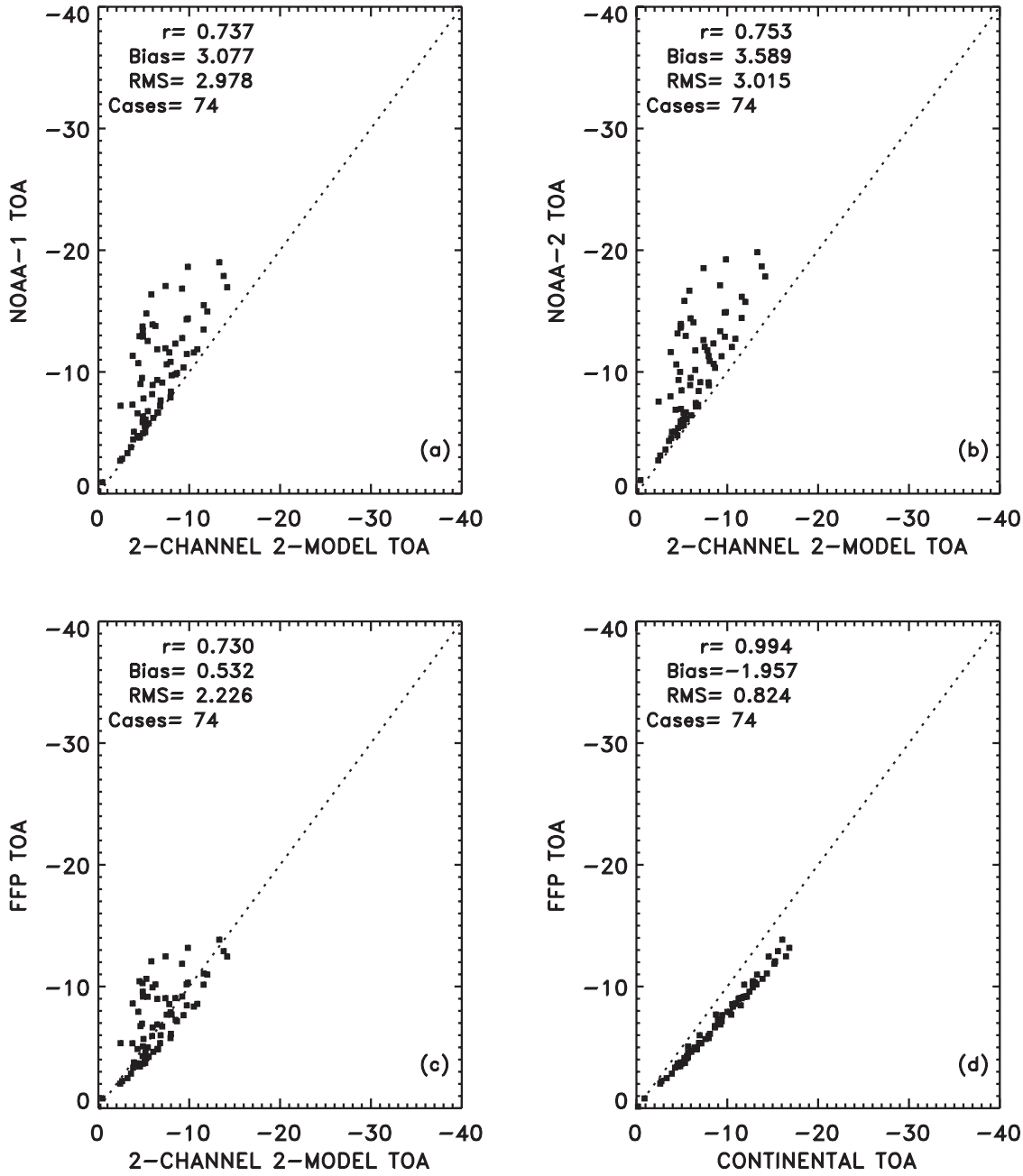

Figure 6. Top of the atmosphere, diurnally averaged, aerosol direct radiative forcing (W m^{-2}) under cloud-free conditions for the cases used in Figure 2. Results for the 2-channel, 2-model scheme are compared with (a) the NOAA Phase 1 model; (b) the NOAA Phase 2 model; and (c) the FFP model. Results for the average continental aerosol model in a single-channel retrieval are compared with the FFP model in (d).

radiative forcing for the NOAA Phase 1 and FFP models are 25–35%, while relative differences in the optical depths retrieved using the two models are 55–60%. The maximum of the relative differences for the top of the atmosphere radiative forcing for the NOAA Phase 2, FFP, and the 2-channel, 2-model retrievals is less than 40%. Of course, the relative lack of sensitivity to aerosol model for the top of the atmosphere radiative forcing does not hold for either the surface or the atmospheric forcing. To obtain the correct surface and atmospheric forcing, the aerosol model used in the retrieval of the optical depth must also absorb the correct amount of sunlight.

[42] The optical depths, top of the atmosphere, and surface cloud-free aerosol direct radiative forcing shown in Figure 7 are consistent with the sensitivities given in Table 2. Slight differences result from departures of the observing dates from the 1 March date used in Table 2, from allowance for small but systematic variations in the radiative forcing sensitivity with latitude, and from the dependence of the sensitivity on optical depth. The average top of

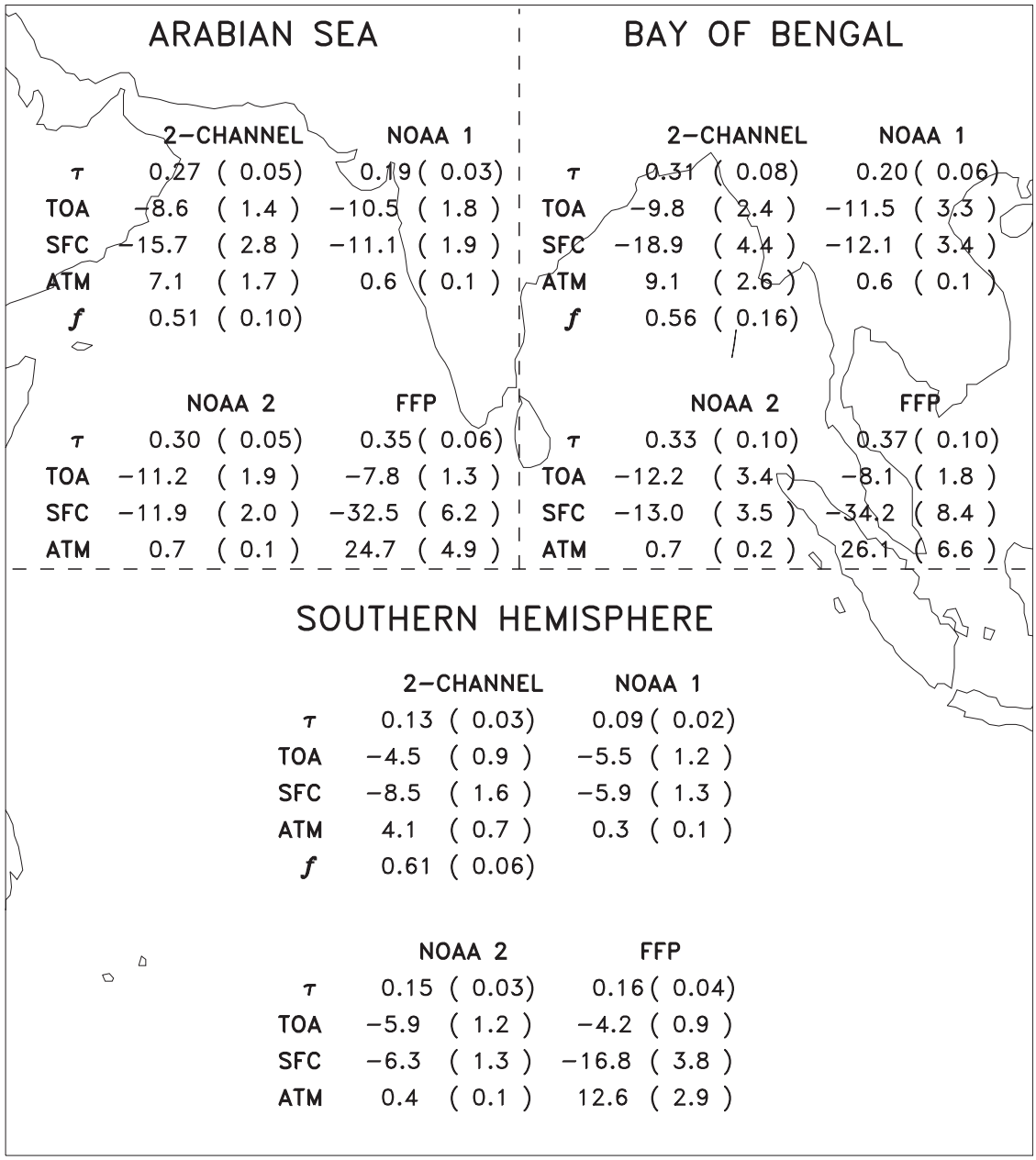

Figure 7. 8-day average and standard deviation of the daily regional averages (parentheses) of aerosol 0.55-μm optical depth, aerosol mixing fraction, *f*, and the direct radiative forcing (W m^{-2}) for the top of the atmosphere (TOA), surface (SFC), and atmosphere (ATM) under cloud-free conditions for the Arabian Sea, Bay of Bengal, and the Indian Ocean in the Southern Hemisphere. The 8 days were sampled from the February−March 1999 INDOEX IFP.

the atmosphere and surface radiative forcing obtained with the 2-channel, 2-model scheme is clearly a mixture of the radiative forcing obtained with the average continental and tropical marine models. The sensitivity of the top of the atmosphere direct radiative forcing per unit 0.55-μm optical depth obtained with the 2-channel, 2-model retrieval lies between −32 and −35 W m^{-2}, while that for the FFP model lies between −22 and −26 W m^{-2}. The larger sensitivities are associated with the results for the Southern Hemisphere where the optical depths are smaller. The empirically derived value obtained by *Satheesh and Ramanathan* [2000] is −25 W m^{-2} per unit 0.5-μm optical depth based on observations at KCO in the Arabian Sea. Satheesh and Ramanathan derived this value by correlating surface measurements of aerosol optical depths with top of the atmosphere radiative fluxes derived from the Clouds and Earth's Radiant Energy System (CERES) radiometer on the Tropical Rain Measurement Mission (TRMM) satellite. The sensitivity per unit 0.55-μm optical depth of the surface forcing for the 2-channel, 2-model scheme lies between −58 and −65 W m^{-2}, less than the −70 to −75 W m^{-2} range deduced empirically by *Satheesh and Ramanathan* [2000], which in turn, is less than the −92 to −105 W m^{-2} range obtained for the FFP model. For both the 2-channel,

Table 3. Composite Regional Means and Standard Deviations of the Daily Regional Means for 8 Days Sampled From February and March 1999[a]

Parameter	Arabian Sea	Bay of Bengal	Southern Hemisphere
Optical depth	0.27 (0.05)	0.31 (0.08)	0.13 (0.03)
f	0.51 (0.10)	0.56 (0.16)	0.61 (0.06)
	Frequencies of Occurrence		
Cloud-free pixels	0.23 (0.06)	0.13 (0.04)	0.08 (0.02)
Overcast pixels	0.01 (0.01)	0.02 (0.01)	0.04 (0.01)
Partly cloudy pixels	0.76 (0.06)	0.85 (0.04)	0.88 (0.03)
Regions containing upper level clouds, but not overcast	0.18 (0.06)	0.39 (0.09)	0.31 (0.08)
Regions overcast by upper level clouds	0.03 (0.01)	0.17 (0.08)	0.11 (0.06)
	Low-Level Cloud Properties		
Cloud cover, partly cloudy pixels	0.41 (0.03)	0.50 (0.07)	0.50 (0.06)
Reflectance, overcast pixels	0.27 (0.09)	0.57 (0.12)	0.47 (0.02)
	Radiative Forcing, W m^{-2}		
	Cloud-Free		
TOA	−8.6 (1.4)	−9.8 (2.4)	−4.5 (0.9)
Surface	−15.7 (2.8)	−18.9 (4.4)	−8.5 (1.6)
	Average-Low		
TOA	−4.5 (0.8)	−3.0 (1.2)	−1.4 (0.2)
Surface	−10.3 (1.8)	−7.4 (2.9)	−3.7 (0.6)
	Average-High		
TOA	−5.5 (0.9)	−4.9 (1.9)	−2.1 (0.2)
Surface	−12.5 (2.2)	−12.0 (4.3)	−5.3 (0.6)
	Average-Zero, All Clouds		
TOA	−4.6 (0.8)	−3.1 (1.2)	−1.5 (0.2)
Surface	−8.4 (1.6)	−6.0 (2.4)	−2.9 (0.5)

[a]As described in the text, "Average Low," "Average High," and "Average-Zero, All Clouds," refer to extreme estimates of the radiative forcing under average cloud conditions.

2-model scheme and the FFP aerosol model, the atmospheric absorption due to the aerosol in the Southern Hemisphere is unrealistic given the lack of absorption found in the in situ aircraft and shipboard observations for the Southern Hemisphere [*Clarke et al.*, 2002; *Quinn et al.*, 2002].

[43] Table 3 gives the diurnally averaged aerosol direct radiative forcing under average cloud conditions for the three regions shown in Figure 7. The results are for the same 8-day sample used to obtain the results shown in the figure. The values in parentheses are the standard deviations of the daily means for the regions. As discussed earlier, the diurnally averaged forcing is calculated by taking the aerosol properties and cloud conditions constant at the values deduced from the NOAA-14 afternoon observations and performing radiative transfer calculations for the variation of the incident sunlight associated with the date and latitude of the observations.

[44] Table 3 also gives the cloud conditions in terms of the quantities described in section 3. In particular, the table gives the average 0.64-μm reflectances for the AVHRR fields of view found to be overcast by optically thick, low-level, layered clouds, and the estimate of the cloud cover for partly cloudy pixels obtained using an average value of 0.44 for the overcast reflectance. As discussed in section 3, the aerosol direct radiative forcing is set to zero for all 1° × 1° latitude-longitude regions found to be overcast by upper-level clouds. In addition, two methods were used to estimate the aerosol direct radiative forcing in regions where upper-level clouds were present but failed to completely cover the region. In one method, the radiative forcing was set to zero, referred to as "Average Low." In the second, the radiative forcing was averaged only for regions that contained no upper-level clouds. Regions that contained upper-level clouds, but were not overcast by the upper-level clouds, were then given the average forcing that was obtained for the regions that contained no upper-level clouds. This estimate is referred to as "Average High." Table 3 also contains estimates in which the radiative forcing was set to zero for all regions containing upper-level clouds and for portions of regions overcast by low-level clouds, referred to as "Average-Zero, All Clouds." Relative differences between "Average High" and "Average Low" were 50% for the top of the atmosphere radiative forcing. Because the mixing fractions of the average continental and tropical marine aerosols were nearly equal, and because the top of the atmosphere radiative forcing for the two models is nearly equal in magnitude, but opposite in sign for scenes overcast by low-level clouds, the top of the atmosphere forcing obtained by setting the forcing to zero for all 1° × 1° latitude-longitude regions that contained upper-level clouds and for all fractions of regions overcast by low-level clouds, "Average-Zero, All Clouds," fell close to that obtained for the "Average Low" estimates. The relative difference between "Average High" and "Average-Zero, All Clouds" reached nearly 70% for the aerosol direct radiative forcing at the surface. In all cases, the magnitude of the surface forcing obtained by setting the forcing to zero

for either upper or low-level clouds is too small. As indicated by the results in Table 2, while clouds diminish the surface forcing somewhat, the resulting forcing remains a sizable fraction of that for cloud-free conditions. The range in values for the forcing given in Table 3 provides an estimate of the uncertainty that arises through the inability to characterize cloud conditions and the effect of the clouds on the aerosol direct radiative forcing.

6. Conclusions

[45] A new aerosol retrieval scheme was developed to take advantage of both the visible and near infrared reflectances measured by the AVHRR. The reflected sunlight was taken to be a composite of the components contributed by two distinctly different aerosol types. The types chosen for this investigation were the average continental and tropical marine aerosol models described by *Hess et al.* [1998]. The models were chosen in part because they represented the polluted continental haze and the marine aerosols that were expected to be found in the INDOEX region and in part because reflectances calculated for cloud-free ocean scenes with these aerosol types occupied the largest portion of the visible and near infrared reflectance domain spanned by any combination of realistic aerosol types (Figure 1). Larger portions of the reflectance domain could be spanned by invoking aerosol models with smaller particles, such as the NOAA Phase 1 model, but particle sizes for this model (Table 1) are much smaller than those found in INDOEX [*Satheesh et al.*, 1999; *Clarke et al.*, 2002; *Quinn et al.*, 2002]. The fraction of the aerosol component contributing to the observed reflectance was determined from the slope of the departures in the near infrared and visible reflectances from their cloud-free and aerosol-free values for ocean scenes. The optical depth of the mixed aerosol was then derived from the departure of the reflectances from their cloud-free and aerosol-free values. For comparison, optical depths were also retrieved using a variety of aerosol models: the INDOEX FFP model described by *Rajeev et al.* [2000], the NOAA Phase 1 and Phase 2 models described by *Stowe et al.* [1997], and the average continental and tropical marine aerosols taken separately in the commonly used single-channel, single-aerosol model retrieval [*Stowe et al.*, 1997; *Rajeev et al.*, 2000] as well as in a two-channel variant of the single-aerosol model retrieval.

[46] Optical depths retrieved at visible and near infrared wavelengths were compared with collocated surface measurements (Figures 2–4). Except for the NOAA Phase 1 model, the comparisons indicated that there was little reason to choose one retrieval scheme or one aerosol model over the other. Biases in the 0.65-μm optical depths were typically less than 0.05 and RMS differences about the bias were typically less than 0.06. Such values are comparable to the bias expected for cloud contamination in the fields of view used to retrieve aerosol properties.

[47] Despite the relatively good agreement between retrieved visible and near infrared optical depths and those measured at the surface, ratios of the retrieved near infrared to visible optical depths compared poorly with the ratios derived from the surface observations (Figure 5). Furthermore, even though the average continental and tropical marine aerosol models were chosen to span the widest possible domain of visible and near infrared reflectances, 50–60% of the reflectances for cloud-free ocean scenes fell outside of the expected domain. All components of the retrieval scheme could contribute to the failure of the reflectances to fall within the expected domain: calibration of the AVHRR, cloud screening, errors in atmospheric corrections, errors in the model used to estimate reflection by the ocean, inappropriate models for the aerosols, etc. Why such a large fraction of the reflectances fall outside the expected domain remains an unsolved problem.

[48] Estimates of the top of the atmosphere and surface aerosol direct radiative forcing were made using the retrieved optical depth and aerosol component mixing fraction in radiative transfer calculations of the shortwave fluxes. For the top of the atmosphere forcing under cloud-free conditions, the derived forcing was relatively insensitive to the choice of aerosol model and retrieval scheme used to derive the aerosol properties. For example, even though the relative differences in the optical depths retrieved using the NOAA Phase 1 and FFP models were 55–60%, the relative differences in the estimates of the top of the atmosphere radiative forcing for cloud-free conditions were 25–35%. The maximum in the relative differences for the top of the atmosphere aerosol direct radiative forcing was 40% for the aerosol models and retrieval schemes used in this study.

[49] *Satheesh and Ramanathan* [2000] obtained empirical estimates for the sensitivity of the top of the atmosphere and surface net solar radiative fluxes for cloud-free conditions at KCO. For the top of the atmosphere cloud-free forcing, the results in Figure 7 and Table 3 suggest that the FFP model underestimates the sensitivity of the radiative forcing by 10% while the 2-channel, 2-model retrieval scheme overestimates the radiative forcing by 30% when compared with the value (-25 W m^{-2} per unit 0.5-μm optical depth) given by *Satheesh and Ramanathan* [2000]. The 2-channel, 2-model, retrieval scheme underestimates the surface forcing by less than 20% while the FFP model overestimates the forcing by 30% when compared to the empirical estimate (-70 to -75 W m^{-2} per unit 0.5-μm optical depth).

[50] Extreme estimates were offered for the aerosol direct radiative forcing under average cloud conditions. For the lower estimate, "Average Low," the forcing was set to zero in $1^\circ \times 1^\circ$ latitude-longitude regions that contained upper-level clouds. For the upper estimate, "Average High," the forcing for regions that contained upper-level clouds was set to the average forcing obtained when no upper-level clouds were present. Relative differences between the upper and lower estimates reached 50% for the top of the atmosphere aerosol direct radiative forcing. By setting the forcing to zero for all $1^\circ \times 1^\circ$ latitude-longitude regions that contained upper-level clouds and all portions of the regions overcast by low-level clouds, "Average-Zero, All Clouds," the resulting top of the atmosphere forcing was almost identical to that obtained by the "Average Low" estimate. Because all but very thick clouds fail to completely attenuate the effect of the aerosols on the solar radiative flux at the surface, the magnitude of the forcing estimated here is likely to be too low, especially for the "Average-Zero, All Clouds" estimate. Relative differences between "Average High" and "Average-Zero, All Clouds" estimates of the aerosol direct radiative forcing at the surface reached 70%.

[51] **Acknowledgments.** This work was supported in part by the National Science Foundation (NSF), ATM-9612886, the Center for Clouds, Chemistry, and Climate at the Scripps Institution of Oceanography, an NSF Science and Technology Center, and NASA NAS1-98140 through the NASA CERES Project.

References

Clarke, A. D., P. K. Quinn, and J. Ogren, INDOEX aerosol: A comparison and summary of chemical, microphysical, and optical properties observed from land, ship, and aircraft, *J. Geophys. Res.*, *107*, 10.1029/2001JD000572, in press, 2002.

Cox, C., and W. Munk, Measurements of the roughness of the sea surface from the sun's glitter, *J. Opt. Soc. Am.*, *44*, 838–850, 1954.

Durkee, P., F. Pfeil, E. Frost, and E. Shima, Global analysis of aerosol particle characteristics, *Atmos. Environ., Part A*, *25*, 2457–2471, 1991.

Haywood, J. M., D. L. Roberts, A. Slingo, J. M. Edwards, and K. P. Shine, General circulation model calculations of the direct radiative forcing by anthropogenic sulfate and fossil-fuel soot aerosol, *J. Clim.*, *10*, 1562–1577, 1997.

Hess, M., P. Koepke, and I. Schult, Optical properties of aerosols and clouds: The software package OPAC, *Bull. Am. Meteorol. Soc.*, *79*, 831–844, 1998.

Higurashi, A., and T. Nakajima, Development of a two channel aerosol retrieval algorithm on global scale using NOAA/AVHRR, *J. Atmos. Sci.*, *56*, 924–941, 1999.

Holben, B. N., et al., AERONET—A federated instrument network and data archive for aerosol characterization, *Remote Sens. Environ.*, *66*, 1–16, 1998.

Houghton, J. T., *The Physics of the Atmosphere*, Cambridge Univ. Press, New York, 1989.

Jayaraman, A., S. K. Satheesh, A. P. Mitra, and V. Ramanathan, Latitude gradient in aerosol properties across the Inter Tropical Convergence Zone: Results from the joint Indo-US study onboard *Sagar Kanya, Curr. Sci.*, *80*, 128–137, 2001.

Kahn, R., P. Banerjee, and D. McDonald, Sensitivity of multiangle imaging to natural mixtures of aerosols over oceans, *J. Geophys. Res.*, *106*, 18,219–18,238, 2001.

Kratz, D. P., The correlated *k*-distribution technique as applied to the AVHRR channels, *J. Quant. Spectrosc. Radiat. Transfer*, *53*, 501–517, 1995.

Lacis, A. A., and J. E. Hansen, A parameterization for the absorption of solar radiation in the Earth's atmosphere, *J. Atmos. Sci.*, *31*, 118–133, 1974.

Loeb, N. G., In-flight calibration of NOAA AVHRR visible and near-IR bands over Greenland and Antarctica, *Int. J. Remote Sens.*, *18*, 477–490, 1997.

McClatchey, R. A., R. W. Fenn, J. E. A. Selby, F. E. Volz, and J. S. Garing, Optical properties of the atmosphere, *Environ. Res. Pap. 411*, U.S Air Force Cambridge Res. Lab., Bedford, Mass., 1972.

Mischenko, M. I., I. V. Geogdzhayev, B. Cairns, W. B. Rossow, and A. A. Lacis, Aerosol retrievals over the ocean by use of channels 1 and 2 AVHRR data: Sensitivity analysis and preliminary results, *Appl. Opt.*, *38*, 7325–7341, 1999.

Pendorf, R., Tables of the refractive index for standard air and the Rayleigh scattering coefficient for the spectral region between 0.2 and 20.0 μm and their application to atmospheric optics, *J. Opt. Soc. Am.*, *47*, 176–182, 1957.

Quinn, P. K., D. J. Coffman, T. S. Bates, T. L. Miller, J. E. Johnson, E. J. Welton, C. Neususess, M. Miller, and P. Sheridan, Variability in aerosol optical properties during INDOEX and controlling factors, *J. Geophys. Res.*, *107*, 10.1029/2000JD000037, in press, 2002.

Rajeev, K., V. Ramanathan, and J. Meywerk, Regional aerosol distribution and its long-range transport over the Indian Ocean, *J. Geophys. Res.*, *105*, 2029–2043, 2000.

Ramanathan, V., et al., Indian Ocean Experiment: An integrated analysis of the climate forcing and effects of the great Indo-Asian haze, *J. Geophys. Res.*, *106*, 28,371–28,398, 2001.

Satheesh, S. K., V. Ramanathan, X. Li-Jones, J. M. Lobert, I. H. Podgorny, J. M. Prospero, B. N. Holben, and N. G. Loeb, A model for the natural and anthropogenic aerosols over the tropical Indian Ocean derived from Indian Ocean Experiment data, *J. Geophys. Res.*, *104*, 27,421–27,440, 1999.

Satheesh, S. K., and V. Ramanathan, Large differences in tropical aerosol forcing at the top of the atmosphere and Earth's surface, *Nature*, *405*, 60–63, 2000.

Stamnes, K., S.-C. Tsay, W. Wiscombe, and K. Jayaweera, A numerically stable algorithm for discrete-ordinate-method radiative transfer in multiple scattering and emitting layered media, *Appl. Opt.*, *27*, 2502–2509, 1988.

Stowe, L. L., A. M. Ignatov, and R. R. Singh, Development, validation, and potential enhancements to the second-generation operational aerosol product at the National Environmental Satellite, Data, and Information Service of the National Oceanic and Atmospheric Administration, *J. Geophys. Res.*, *102*, 16,923–16,934, 1997.

Tahnk, W. R., and J. A. Coakley Jr., Improved calibration coefficients for NOAA-14 AVHRR visible and near-IR channels, *Int. J. Remote Sens.*, *22*, 1269–1283, 2001a.

Tahnk, W. R., and J. A. Coakley Jr., Updated calibration coefficients for NOAA-14 AVHRR channels 1 and 2, *Int. J. Remote Sens.*, *22*, 3053–3057, 2001b.

Tahnk, W. R., and J. A. Coakley Jr., Aerosol optical depths and direct radiative forcing for INDOEX derived from AVHRR: Observations, January–March 1996–2000, *J. Geophys. Res.*, *107*, 10.1029/2000JD000183, in press, 2002.

Wang, M., and H. R. Gordon, Estimating aerosol optical properties over the oceans with the multiangle imaging spectroradiometer: Some preliminary results, *Appl. Opt.*, *33*, 4042–4057, 1994.

Wielicki, B. A., and L. Parker, On the determination of cloud cover from satellite sensors: The effect of sensor spatial resolution, *J. Geophys. Res.*, *97*, 12,799–12,823, 1992.

J. A. Coakley Jr. and W. R. Tahnk, College of Oceanic and Atmospheric Sciences, Ocean Admin 104, Oregon State University, Corvallis, OR 97331-5503, USA. (coakley@coas.oregonstate.edu)

A. Jayaraman, Planetary Atmospheric Sciences Division, Physical Research Laboratory, Navrangpura Ahmedabad, -380 009, India.

P. K. Quinn, NOAA/Pacific Marine Environmental Laboratory, Seattle, WA 98115, USA.

C. Devaux and D. Tanré, Laboratoire d' Optique Atmosphérique, CNRS Université des Sciences et Technologies de Lille Villeneuve d' Ascq, France.